DCA promotes a novel tolerogenic program in CD4$^+$ T cells by inhibiting CDK8

Azlann Arnett[1], Keagan G Moo[1], Kaitlin J Flynn[1], Thomas B Sundberg[2], Liv Johannessen[3], Alykhan F Shamji[2], Nathanael S Gray[3], Thomas Decker[4], Vivian H Gersuk[1], David E Levy[5], Isabelle J Marié[5], Ziaur S Rahman[6], Ye Zheng[7], Peter S Linsley[1], Ramnik J Xavier[8,9], Bernard Khor[1]

[1]Benaroya Research Institute, Seattle, WA, USA. [2]Center for the Science of Therapeutics, Broad Institute, Cambridge, MA, USA. [3]Department of Biological Chemistry and Molecular Pharmacology, Harvard Medical School, Boston, MA, USA. [4]Max Perutz Labs, University of Vienna, Vienna, Austria. [5]Department of Pathology, New York University School of Medicine, New York, NY, USA. [6]Department of Microbiology and Immunology, Pennsylvania State University College of Medicine, Hershey, PA, USA. [7]NOMIS Center for Immunobiology and Microbial Pathogenesis, Salk Institute for Biological Studies, La Jolla, CA, USA. [8]Center for Computational and Integrative Biology, Massachusetts General Hospital, Harvard Medical School, Boston, MA, USA. [9]The Broad Institute of Massachusetts Institute of Technology and Harvard, Cambridge, MA, USA.

Abstract

Immune health requires innate and adaptive immune cells to engage precisely balanced pro- and anti-inflammatory forces. A holistic understanding of how individual small molecules affect this balance is essential to anticipate immune-related side effects, select mitigating immunomodulatory therapies and highlight novel utility as immunomodulators. We previously showed that the high-specificity, low-toxicity cyclin dependent kinase 8 (CDK8) inhibitor DCA promotes tolerogenic effects in innate immune cells. Here, we demonstrate that DCA exerts a novel profile of tolerogenic activity on $CD4^+$ T cells, promoting T_{reg} and Th2 while inhibiting Th1 and Th17 differentiation. DCA enhances human T_{reg} differentiation and our models demonstrate clear tolerogenic function of DCA-driven T_{reg}s in the absence of confounding contribution from DCA-innate immune interactions. DCA engages unique mechanisms, including specifically enhancing early Foxp3 expression via regulating c-Jun phosphorylation, to promote T_{reg} differentiation. CDK8 inhibitors are currently being developed to treat cancer; our findings suggest that the potential blunting of host-versus-tumor effects may warrant ancillary pro-inflammatory agents. Importantly, these results highlight novel utility of DCA as an immunomodulator, not only in vivo, but also in ex vivo cellular therapy.

Introduction

The immune system comprises innate and adaptive immune cells whose collaborative and coordinated responses are required to maintain the healthy state. Each cell type can exert either pro- or anti-inflammatory forces. For example, innate immune cells can secrete either pro- (e.g. IFNγ) or anti- (e.g. IL-10) inflammatory cytokines while $CD4^+$ T cells can differentiate into either pro- (e.g. Th1, Th17) or anti- (T_{reg}) inflammatory subsets (1-5). These pro- and inflammatory forces must be precisely balanced; dysregulation of this balance can predispose to autoimmunity, infection or cancer (3, 6). Patients and murine models demonstrate that defects in individual cell types can lead to disease. Therefore, it is important to holistically understand how individual genes and therapies affect both innate and adaptive immune responses. This understanding is essential to restore immune homeostasis in any given patient and to anticipate immunomodulatory side effects of current therapies.

We have previously demonstrated how small molecules can highlight novel pathways of immunoregulation in primary immune cells. For example, we showed that small molecule inhibition of the dual-specificity tyrosine phosphorylation-regulated kinase 1A (DYRK1A) promotes differentiation of murine and human $CD4^+$ T cells into T_{reg}s (7). We also showed that small molecule inhibition of salt-induced kinases (SIKs) enhanced production of IL-10 by murine and human myeloid cells (8). However, a comprehensive understanding of how both innate and adaptive immune cell function is modulated remains lacking for most small molecules.

Here, we investigate the effect of the natural product-derived small molecule dihydro-cortistatin A (DCA) on murine and human $CD4^+$ T cells. We previously found that DCA promotes production of IL-10 in myeloid cells by inhibiting cyclin-dependent kinase 8 (CDK8) (9-11). CDK8 is an essential component of the CDK8 submodule of the Mediator coactivator complex, which regulates RNA polymerase II activity (12, 13). The CDK8 submodule facultatively binds the Mediator complex, phosphorylates transcription factors and regulates specific pathways (13-15).

CDK8 phosphorylates several transcription factors important in many immune cells, including $STAT1^{Ser727}$, $STAT3^{Ser727}$ and the AP-1 family member c-Jun (16-19). Consistent with this, growing evidence suggests that CDK8 regulates both innate and adaptive immune responses. We previously showed that c-Jun phosphorylation by CDK8 regulates IL-10 production in innate immune cells (11). Deletion of CDK8 in NK cells enhances cytotoxicity and improves tumor surveillance (20, 21). Furthermore, CDK8/19 inhibitors promote T_{reg} differentiation (22, 23). These findings highlight the importance of better understanding which immune processes are regulated by CDK8 inhibition, and how. In particular, recent studies pointing to DCA as the CDK8 inhibitor with highest specificity and lowest toxicity highlight DCA as a particularly important compound to investigate (24).

Here, we demonstrate that DCA exerts a unique pattern of immunomodulation compared to other known immunomodulatory small molecules. Using both small molecule inhibitors and CRISPR/Cas9 knockdown, we find that DCA works by disrupting CDK8 to promotes the differentiation of T_{reg} and Th2 cells while inhibiting the differentiation of pro-

inflammatory subsets including Th1 and Th17. We show that DCA-driven T_{reg}s are fully suppressive in the absence of concomitant tolerogenic effects on innate immune cells. DCA works through a novel mechanism of enhancing early *Foxp3* expression, which our data suggest involves modulation of c-Jun activity. These findings highlight a novel immunomodulatory role for DCA in broadly driving tolerogenic programs in both innate and adaptive immune cells while inhibiting pro-inflammatory programs in $CD4^+$ T cells. These findings are discussed in the context of implications to future therapeutic use of CDK8 inhibitors.

Results

DCA exerts tolerogenic effects on murine and human $CD4^+$ T cell differentiation. Given our previous observation that DCA promotes tolerogenic IL-10 production in innate immune cells, we determined whether DCA exerts tolerogenic effects on $CD4^+$ T cell differentiation (11). We tested the effect of DCA on naïve murine $CD4^+$ T cells cultured in suboptimal pro-T_{reg} or -Th2 conditions (T_{reg}^{low} and $Th2^{low}$, respectively) as we previously described (7). DCA enhanced differentiation of both T_{reg} and Th2 cells (Fig. 1A). DCA increased T_{reg}s specifically in cultures of FACS-sorted naïve $CD4^+$ T cells, but not sorted T_{reg}s, further demonstrating that the increase in T_{reg}s is due to enhanced differentiation of T_{reg}s rather than expansion of existing T_{reg}s (Supplemental Fig. 1A). To examine if these tolerogenic effects extended to inhibiting differentiation of pro-inflammatory T cell lineages, we tested how DCA impacts murine T cells cultured in near-optimal pro-Th1 and -Th17 conditions ($Th1^{hi}$ and $Th17^{hi}$, respectively). DCA inhibited differentiation of Th1 and Th17 cells by >50% (Fig. 1A). Notably, DCA promoted differentiation of T_{reg} and Th2 cells even in near-optimal $Th17^{hi}$ and $Th1^{hi}$ conditions respectively (Fig. 1A, FACS plots). In the context of non-polarizing Th0 conditions, DCA significantly, albeit modestly, enhanced murine T_{reg} and Th2 differentiation (Fig. 1B). Th1 differentiation was slightly reduced below the level of statistical significance and Th17 cells were too infrequent to accurately assess (Fig. 1B). These results suggest that DCA can enhance T_{reg}/Th2 differentiation even with very low levels of cytokine that may be present in media (e.g. TGFβ) or produced stochastically (e.g. IL-4). Therefore, DCA exerts powerful tolerogenic effects on murine T cell differentiation.

We further investigated whether DCA similarly affects human T_{reg} differentiation by using human $CD4^+$ T cells cultured in suboptimal (human-specific) T_{reg}^{low} conditions. DCA treatment enhanced the total number and percentage of human T_{reg}s, similar to our observations in murine cells (Fig. 1C-D). We next sought to benchmark the pro-T_{reg} effect of DCA against the well-described T_{reg} enhancers all-trans retinoic acid (ATRA) and rapamycin (Rapa) (25-31). In murine and human $CD4^+$ T cells cultured in suboptimal T_{reg}^{low} conditions, DCA treatment enhanced the total number of T_{reg}s significantly higher than either ATRA or rapamycin (Fig. 1C). In addition, DCA enhanced the percentage of T_{reg}s to a level similar to ATRA and rapamycin (Fig. 1D). These results highlight that DCA potently enhances T_{reg} differentiation in both murine and human T cells.

DCA identifies a novel chemical immunophenotype secondary to CDK8 inhibition. To generate a more holistic view of how DCA impacts T cell differentiation, we investigated the dose-response of murine $CD4^+$ T cells to DCA and two other tolerogenic small molecules in the

context of suboptimal pro-T_{reg}, Th2, Th1 and Th17 conditions (T_{reg}^{low}, $Th2^{low}$, $Th1^{low}$ and $Th17^{low}$, respectively) (7). These experiments showed that DCA enhanced differentiation of both murine T_{reg} and Th2 cells with identical EC_{50}, supporting the involvement of a common mechanistic target (Fig. 2A). The EC_{50} of the pro-T_{reg} effect was similar to the EC_{50} we previously found for enhancing IL-10 production in bone marrow-derived dendritic cells, suggesting a similar mechanism of action (11). To understand if compounds that enhance T_{reg} differentiation also typically enhance Th2 differentiation, we tested the DYRK1A inhibitor harmine, which we previously demonstrated to enhance T_{reg} and inhibit Th17, and to a lesser extent Th1, differentiation (7). Harmine did not enhance differentiation of Th2 cells (Fig. 2A). Conversely, to understand if compounds that exert tolerogenic effects on innate immune cells typically enhance T_{reg} and Th2 differentiation, we tested the multi-kinase inhibitor HG-9-91-01 that potently targets salt-inducible kinase (SIK) 1-3, which we previously showed enhances IL-10 production in bone marrow-derived dendritic cells (BMDCs) (8). Inhibiting SIK1-3 did not enhance differentiation of naïve murine $CD4^+$ T cells towards any Th lineage, consistent with innate cell-specific tolerogenic effects (Fig. 2A). Therefore, DCA, HG-9-91-01 and harmine appear to induce distinct immune phenotypic profiles, which we term chemical immunophenotypes, reflecting distinct pathways regulating tolerogenicity in innate and adaptive immune cells.

We and others have previously shown that DCA inhibits CDK8 kinase activity with immunomodulatory effects (11, 20-23). We used two different approaches to validate CDK8 as the T_{reg}-relevant mechanistic target of DCA. Firstly, we tested DCA side-by-side with a structurally distinct small molecule CDK8 inhibitor, BRD-6989 (11). In T_{reg}^{low} conditions, both CDK8 inhibitors showed concentration-dependent enhancement of murine T_{reg} differentiation with concentrations that induce half-maximal effects (EC_{50}) for each compound similar to that observed for enhancing IL-10 production in BMDCs (Fig. 2B) (11). The EC_{50} of DCA was much lower than of BRD-6989, driving its subsequent preferential use (Fig. 2B). Notably, DCA and BRD-6989 both exhibited low cytotoxicity, even less than that observed with harmine, which we previously identified as one of the least cytotoxic T_{reg} enhancers (Fig. 2B) (7). Secondly, we used CRISPR/Cas9 to knock out *CDK8* in primary human $CD4^+$ T cells, which led to increased T_{reg} differentiation compared to control cells edited at the IgA locus (Fig. 2C and Supplemental Fig. 1B). These results indicate that DCA enhances murine and human T_{reg} differentiation by inhibiting CDK8.

DCA-driven T_{reg}s are fully tolerogenic in the absence of innate immune tolerogenic effects. We next interrogated the suppressive capacity of DCA-driven T_{reg} cells both in vitro and in vivo. Using a standard in vitro suppression assay, we observed no significant differences in the ability of T_{reg}^{hi}- or T_{reg}^{DCA}-driven murine T_{reg} cells to suppress proliferation of co-cultured responder $CD4^+$ T cells (Figure 3A, red and blue lines respectively). We tested the capacity of DCA-driven T_{reg}s to inhibit inflammation in vivo using a murine model of type 1 diabetes. In this model, transfer of NOD-*BDC2.5*$^+$ $CD4^+$ T cells, specific for an epitope derived from the islet antigen chromogranin A, into NOD-*scid* recipients results in islet β-cell destruction and onset of diabetes about 10 days later (Fig. 3B, black line) (32, 33). Co-injection of antigen-specific T_{reg} cells, generated from naïve NOD-*BDC2.5.Foxp3*$^{IRES\text{-}GFP}$ $CD4^+$ T cells using either T_{reg}^{DCA} or T_{reg}^{hi}

conditions, significantly and similarly delayed onset of diabetes (Fig. 3B, blue and red lines respectively) (7). Finally, we observed similar results in a murine model of intestinal inflammation where transfer of CD45RB^{hi}CD4^{+} T cells into B10.RAG2$^{-/-}$ recipients resulted in expansion of donor T cells and inflammation most prominent in the colon about 4 weeks later (Fig. 3C, black line) (34, 35). Transfer of T_{reg} cells, generated from naïve wild-type C57Bl/6 CD4^{+} T cells using either T_{reg}^{DCA} or T_{reg}^{hi} conditions, resulted in significant and similar delay of onset of intestinal inflammation (Fig. 3C, blue and red lines respectively) (36). Together, these results demonstrate that DCA-driven T_{reg} cells are fully functional and equivalent to T_{reg}^{hi}-generated T_{reg} cells both in vitro and in vivo, using model systems employing different genetic backgrounds and T cell specificities. Importantly, these experiments demonstrate that DCA exerts a strong T_{reg}-intrinsic tolerogenic effect in the absence of concomitant effects on the innate immune compartment.

DCA exerts tolerogenic effects on T cell differentiation independently of STAT1/STAT3 Ser727 phosphorylation. CDK8 phosphorylates STAT1 and STAT3 on Ser727 in several cell types (37-40). Although the role of Ser727 phosphorylation in Th1/Th17/T_{reg} differentiation is unknown, its potential contribution is suggested by the central role of STAT1^{Tyr701} and STAT3^{Tyr705} tyrosine phosphorylation to Th1 and Th17 differentiation respectively (41-43). We found that DCA reduced IL-6-driven phosphorylation of STAT3^{Ser727} in murine CD4^{+} T cells (Fig. 4A). However, this did not reduce either STAT3^{Tyr705} phosphorylation or expression of the key Th17 transcription factor RORγt (Fig. 4B-C). Total STAT3 protein was only slightly reduced in the context of T cell stimulation (Fig. 4B). To definitively test the role of STAT3^{Ser727} phosphorylation, we examined the effect of DCA on Th17 differentiation in primary CD4^{+} T cells from *Stat3^{Ser727Ala}* mice, in which Ser727Ala mutation prevents STAT3^{Ser727} phosphorylation (38). *Stat3^{Ser727Ala}* CD4^{+} T cells showed reduced Th17 differentiation, highlighting a novel role of STAT3^{Ser727} phosphorylation in this process (Fig. 4D). Importantly, DCA similarly suppressed Th17 differentiation in both *Stat3^{Ser727Ala}* and wild-type CD4^{+} T cells, showing that CDK8 inhibition regulates Th17 differentiation independently of regulating STAT3^{Ser727} phosphorylation (Fig. 4D). DCA similarly enhanced T_{reg} differentiation in both *Stat3^{Ser727Ala}* and wild-type CD4^{+} T cells (Fig. 4E). Together, these results demonstrate that DCA regulates Th17 and T_{reg} differentiation independent of STAT3^{Ser727} phosphorylation.

Similarly, we found that DCA reduced IFNγ-driven phosphorylation of STAT1 on Ser727 but not on Tyr701 in murine CD4^{+} T cells; total STAT1 protein was unaltered (Fig. 4F-G). Expression of the hallmark Th1 transcription factor Tbet was unaltered by DCA except at day 4 (Fig. 4H). We examined the effect of DCA on Th1 differentiation in primary CD4^{+} T cells from *Stat1^{Ser727Ala}* mice, in which Ser727Ala mutation prevents STAT1^{Ser727} phosphorylation (39). *Stat1^{Ser727Ala}* CD4^{+} T cells showed reduced Th1 differentiation, highlighting a novel role of STAT1^{Ser727} phosphorylation in this process (Fig. 4I). Importantly, DCA similarly suppressed Th1 differentiation in both *Stat1^{Ser727Ala}* and wild-type CD4^{+} T cells, showing that CDK8 inhibition regulates Th1 differentiation independently of effects on STAT1^{Ser727} phosphorylation (Fig. 4I). Additionally, DCA similarly enhanced T_{reg} differentiation in both *Stat1^{Ser727Ala}* and wild-type CD4^{+} T cells (Fig. 4J). Together, these results demonstrate that DCA regulates Th1 and T_{reg} differentiation independent of STAT1^{Ser727} phosphorylation.

DCA enhances expression of key T_{reg} transcription factors that work through multiple cis-regulatory elements. To better understand how DCA enhances T_{reg} differentiation, we examined the expression of key T_{reg} transcription factors. DCA enhanced the expression of *Foxp3*, *Eos* and *Helios* in murine $CD4^+$ T cells (Fig. 5A) (44-46). Consistent with the induction of key T_{reg} transcription factors, several other genes were regulated as expected. For example, expression of *Cd25* was upregulated while expression of *Il2* was downregulated (Fig. 5A) (47). This induction of key T_{reg} transcription factors did not involve either enhanced SMAD2/SMAD3 phosphorylation and mTOR inhibition, implying the involvement of novel pathway(s) (Supplemental Fig. 2A-B). Next, to better understand the cis-regulatory elements most important for DCA-mediated FOXP3 enhancement, we examined mice lacking the key regulatory elements of the *Foxp3* locus, CNS1, CNS2 and CNS3 (48). TGFβ titration studies revealed cell-intrinsic roles for all three CNS elements in T_{reg} differentiation in vitro, with CNS 1 ≅ CNS2 > CNS3 (Fig. 5B). DCA enhanced T_{reg} differentiation in cells lacking CNS1, CNS2 or CNS3, although not to the same extent as wildtype $CD4^+$ T cells, and suggested a relative contribution of CNS1 > CNS2 > CNS3 (Fig. 5B and Supplemental Fig. 2C). These results support a mixed model where all three cis-acting elements, particularly CNS1, participate in DCA-regulated mechanisms.

DCA enhances AP-1 activity and early Foxp3 expression. Temporal analysis of FOXP3 expression throughout the period of culture revealed indistinguishable kinetics between T_{reg}^{low} and T_{reg}^{hi} conditions until day 2, with $FOXP3^+$ cells subsequently increasing in T_{reg}^{hi} conditions and decreasing in T_{reg}^{low} conditions (Fig. 6A) (7). Notably, DCA significantly increased $FOXP3^+$ cells until day 2, compared to either T_{reg}^{low} or T_{reg}^{hi} conditions (Fig. 6A). These data suggest that DCA promotes T_{reg} differentiation at least in part by enhancing early expression of FOXP3 and point to the value of including earlier time points in mechanistic analyses of DCA.

To generate an unbiased understanding of how DCA impacts the T_{reg} transcriptional landscape across time, we cultured *Foxp3*^{GFP} $CD4^+$ T cells in T_{reg}^{low}, T_{reg}^{hi} and T_{reg}^{DCA} conditions, and profiled naïve $CD4^+$ T cells, sorted GFP^+ and GFP^- cells at day 2 (all conditions) and sorted GFP^+ T_{reg}s at day 4 (T_{reg}^{hi} and T_{reg}^{DCA} conditions)(Fig. 6A). The largest determinants of variation revealed by principal component (PC) analyses related to T cell activation (PC1, 46.1% of variation) and the mature T_{reg} program (PC2, 18.9% of variation)(Fig. 6B). A small but consistent DCA-related signature was detected in the fourth PC, accounting for 4.1% of variation (Fig. 6C). Compared to the dearth of differentially expressed genes in either $FOXP3^+$ or $FOXP3^-$ cells cultured in T_{reg}^{low} or T_{reg}^{hi} conditions at day 2, DCA treatment detectably, if modestly, altered the transcriptional landscape in all cells examined at day 2 and day 4 (6D and Supplemental Fig. 3). As CDK8 phosphorylates transcription factors, we reasoned that mechanistic insight might be gleaned from understanding the common transcription factor(s) linking the genes dysregulated by DCA. Transcription factor binding site analysis of the genes perturbed by DCA revealed AP-1 as the only transcription factor consistently enriched in genes impacted by DCA in day 2 $FOXP3^-$, day 2 $FOXP3^+$ and day 4 $FOXP3^+$ cells (Fig. 6E). This finding is particularly striking as previous studies have shown that CDK8 inhibition increases AP-1 activity in myeloid cells in part by modulating phosphorylation of the negative regulatory site Ser243 on the AP-1

family member c-Jun (11, 17, 18). Our interrogation of c-Jun in T cells revealed robust and similar induction of phosphorylation on both Ser243 and Ser63 upon stimulation in either T_{reg}^{low} or T_{reg}^{hi} conditions (Fig. 6F). Interestingly, DCA significantly reduced c-Jun phosphorylation on the negative regulatory site Ser243, without significantly affecting phosphorylation on the activating site Ser63 (Fig. 6F). These results imply that CDK8 inhibition promotes T_{reg} differentiation at least in part by modulating c-Jun Ser243 phosphorylation.

Discussion

Here we demonstrate that DCA exerts broad and previously unappreciated tolerogenic effects on $CD4^+$ T cells, promoting differentiation of T_{reg} and Th2 cells, while inhibiting Th1 and Th17 differentiation. Therefore, DCA promotes type 2 and anti-inflammatory immune responses while inhibiting type 1 immune responses. Our use of both novel small molecules (DCA and BRD-6989) and CRISPR/Cas9-mediated deletion point to CDK8 inhibition as the mechanism by which DCA exerts these effects. In conjunction with our previous findings that DCA enhances IL-10 production in myeloid cells, our current data highlight DCA's profile of immunoregulatory activity as distinct from that induced by SIK- and DYRK1A-inhibitors, which exert tolerogenic effects specifically in either innate or adaptive immune cells, but not both (7, 11). These distinct chemical immunotypes point to an important way to classify both probe molecules and drugs, that could inform about potential side effects as well as suggest shared mechanistic pathways, thus guiding both selection of synergistic therapies and precision medicine approaches. Given that CDK8 inhibition exerts anti-inflammatory effects in both adaptive and innate immune cells, it is tempting to speculate that CDK8 regulates evolutionarily older pathways of tolerogenicity conserved between adaptive and innate immunity.

The translational relevance of these data is reinforced by our finding that DCA promotes T_{reg} differentiation in primary human $CD4^+$ T cells. We note that T_{reg}s generated using DCA are fully functional in vitro and in vivo. Importantly, our use of T_{reg}-transfer models specifically interrogates the functionality of DCA-driven T_{reg}s and avoids confounding immunomodulatory effects of DCA-mediated CDK8 inhibition on other cell types, including innate immune cells, that could confound the interpretation of models using systemic drug administration (22, 23). These studies have implications for the anticipated clinical use of CDK8 inhibitors as cancer therapeutics, driven by findings that CDK8 can act as a proto-oncogene (49, 50). The broad tolerogenic effects of DCA may impair host-versus-tumor effects and warrant combination therapy with pro-inflammatory agents. Alternatively, DCA and other CDK8 inhibitors may find utility as tolerogenic immunomodulators. Studies suggesting poor long-term tolerability of CDK8 inhibitors, together with our data showing DCA impacts early pathways in T_{reg} differentiation, support this consideration (51). Importantly, we recognize the utility of DCA in generating T_{reg}s ex vivo, which would circumvent concerns regarding toxicity in vivo (51).

Our studies reveal a novel and unexpected property of DCA enhancing expression of FOXP3 and many FOXP3-regulated genes at early timepoints, with FOXP3 expression at later timepoints decaying at a rate similar to that seen in T_{reg}^{low} conditions. These kinetics of FOXP3 expression are distinct from those observed with T_{reg}^{hi} conditions, where early FOXP3 expression is identical to that observed in T_{reg}^{low} conditions with continued increase in $FOXP3^+$

cells at later timepoints. This suggests a model of T_{reg} differentiation that involves independently regulated early and late pathways. Whereas early pathways might involve TGFβ licensing cells to adopt T_{reg} fate and express FOXP3, later pathways might center on maintaining T_{reg} lineage commitment. Our data support a model where DCA enhances early pathways regulating FOXP3 expression. This suggests particular therapeutic relevance to patients who have corresponding defects in early pathways of T_{reg} differentiation and also raises the possibility of broader tolerogenic utility when used in conjunction with synergistic therapies that enhance late pathways of T_{reg} differentiation.

Our expression profiling studies support that DCA enhances early expression of FOXP3 be regulating AP-1 transcription factors such as c-Jun. Our data demonstrate that DCA specifically reduced phosphorylation of the inhibitory Ser243 of c-Jun. This is in line with previous finding that CDK8 regulates c-Jun^{Ser243} in myeloid cells (11). Our data supports a role for multiple FOXP3 enhancer elements (CNS1, CNS2 and CNS3) in CDK8-regulated expression of FOXP3, suggesting that CDK8 may be recruited to the FOXP3 promoter together with the Mediator complex, subsequently regulating *Foxp3* expression at least in part by phosphorylating c-Jun.

Our findings highlight some of the opportunities and challenges that accompany mechanistic dissection of small molecules in T cell biology. Prior knowledge that CDK8 phosphorylates STAT proteins, which play essential roles in T cell differentiation, suggest CDK8-STAT interactions as prime candidates to explain how CDK8 inhibition regulates T cell differentiation (16). Our experiments using *Stat1*^{Ser727Ala} and *Stat3*^{Ser727Ala} mice clearly demonstrate that CDK8 regulates Th1, Th17 and T_{reg} differentiation independent of STAT1/STAT3 Ser727 phosphorylation. Prior studies suggest that STAT1^{Ser727}/STAT3^{Ser727} phosphorylation is required for full transcriptional activity (37-40). Consistent with this, we demonstrate a novel role of STAT1^{Ser727} and STAT3^{Ser727} phosphorylation in regulating Th1 and Th17 differentiation, identifying this as a new potential therapeutic target in T cells.

Recent studies identify AS2863619 and CCT251921 as CDK8/19 inhibitors that enhance T_{reg} differentiation (22, 23). Our findings that DCA and BRD-6989 enhance T_{reg} differentiation are important not only because they identify additional CDK8/19 inhibitors with similar effects, but also because recent studies point to DCA as having higher specificity and lower toxicity (24). Our studies here show important novel aspects. First, we show that DCA enhances Th2 differentiation. Second, we demonstrate that DCA enhances human T_{reg} differentiation. Third, we highlight mechanistic considerations. We do not see differences in SMAD2/SMAD3 phosphorylation, contrary to Guo et al (22). Whether this is due to compound-specific differences remains to be clarified. Further, our findings show that CDK8-regulated phosphorylation of STAT proteins does not necessarily drive effects on T cell differentiation, pointing to the need to develop STAT5 Ser-Ala mutants to test the role of CDK8-regulated STAT5 phosphorylation advocated by Akamatsu et al (23). Our data demonstrate clearly that DCA enhances early FOXP3 expression. Our data argue for a role of c-Jun, further interrogation of which is of future interest. Fourth, we do not see increased suppressive activity of CDK8 inhibitor-enhanced T_{reg}s, using either DCA or BRD6989 reported by Guo et al (22). Finally, our

use of T_{reg}-transfer models definitively demonstrate T_{reg}-intrinsic effects of DCA in the absence of confounding tolerogenic effects on other cells, including innate immune cells.

In summary, our studies highlight DCA as a novel, human-relevant immunomodulator with potent tolerogenic effects in both innate and adaptive immune cells. DCA's unusual chemical immunophenotype has important mechanistic and therapeutic implications. Our demonstration that DCA effectively enhances T_{reg} differentiation compared to canonical T_{reg} enhancers suggests utility in approaches to generate T_{reg}s ex vivo for adoptive cellular therapy. In addition, the broadly tolerogenic effects of DCA suggest that it may broadly be useful in the setting of pathologic inflammation or autoimmunity.

Mice and Reagents

Balb/c, C57Bl/6, *Foxp3*$^{IRES\text{-}GFP}$, *CD45.1*$^{+/+}$, NOD-*scid* and NOD-*BDC2.5* mice were purchased from Jackson Labs. NOD-*BDC2.5.Foxp3*$^{IRES\text{-}GFP}$ mice were from the JDRF Transgenic Core (Harvard Medical School, Boston, MA). C57Bl/10-*Rag2*$^{-/-}$ mice were a kind gift from Brian Kelsall (35). *Stat1*^{Ser727Ala}, *Stat3*^{Ser727Ala}, *Foxp3*$^{\Delta CNS1\text{-}gfp}$, *Foxp3*$^{\Delta CNS2\text{-}gfp}$ and *Foxp3*$^{\Delta CNS3\text{-}gfp}$ mice were previously described (38, 39, 48). Δ16-cortistatin A (DCA) was a generous gift from P. Baran (The Scripps Research Institute) and synthesized as previously reported (9, 52). Small-molecule reagents were confirmed to have ≥95% purity by HPLC–MS. Antibodies, cytokines, and chemical compounds used are listed in Supplementary file 1.

Murine T cell isolation and culture

Unless otherwise noted, CD4$^+$ CD62L$^+$ naïve T cells were isolated from 8-12 week old mice using CD4 negative enrichment kits (Stemcell Technologies, Vancouver, Canada) and CD62L microbeads (Miltenyi Biotec, San Diego, CA) according to the manufacturer's instructions and confirmed >90% pure by flow cytometry. Cells were cultured on 96 well plates pre-coated with anti-CD3 and anti-CD28 using conditions outlined in Supplementary file 2. The addition of DCA to T_{reg}^{low} conditions is abbreviated as T_{reg}^{DCA}. T_{reg} and Th1 cultures were fed with equal volume of IL-2 supplemented media (20ng/ml) and retreated with compound at day 2, split 1:2 into IL-2-supplemented media (10 ng/ml) at day 3 and analyzed at day 4. Th17 cultures were treated similarly except no IL-2 was supplemented. Th2 cultures were treated similarly as T_{reg} cultures except they were additionally split 1:2 into IL-2 supplemented media (10 ng/ml) at day 4 and day 5 and analyzed on day 6.

Human T cell isolation and culture

Frozen PBMCs and fresh peripheral blood samples were obtained from the Benaroya Research Institute Immune Mediated Disease Registry and Repository. Human peripheral blood mononuclear cells were isolated from fresh whole blood by Ficoll-Paque (GE Healthcare, Little Chalfont, United Kingdom). CD4$^+$CD45RA$^+$ naïve T cells were isolated using negative enrichment kits (Stemcell Technologies, Vancouver, Canada) per manufacturer's instructions and confirmed >90% pure by flow cytometry. Cells were cultured on 96 well plates pre-coated with anti-CD3 and anti-CD28 using conditions outlined in Supplementary file 2. T_{reg} cultures were fed with equal volume of IL-2 supplemented media (20ng/ml) and retreated with compound at day 2, split 1:2 into IL-2-supplemented media (10 ng/ml) at day 4 and analyzed at day 5.

Flow Cytometry

Cells were stimulated with PMA and ionomycin (50 and 500ng/ml respectively) (Sigma Aldrich, St. Louis, MO) in the presence of Golgistop (BD Biosciences, San Jose, CA) 5 hours prior to analysis as necessary. Cells were typically stained with LIVE/DEAD and anti-CD4 prior to fixation and permeabilization, which was generally performed with either Foxp3 fixation/permeabilization buffers (eBioscience, San Diego, CA). Phosflow cell lyse/fix and PermIII buffers (BD Biosciences, San Jose, CA) were used for phospho-protein assessment. Intracellular staining was performed per manufacturer's instructions. Counting beads (10 µm, Spherotech, Lake Forest, IL) were added at 5000 per sample. Acquisition was performed on either a FACScalibur or a FACScanto (BD Biosciences, San Jose, CA). Cell sorting was performed

using a FACs Aria II (BD Biosciences, San Jose, CA). Data was analyzed using FlowJo software (Treestar, Ashland, OR). Fractional maximal enhancement was determined by increase in percentage lineage-committed cells, relative to maximal cytokine-driven enhancement as previously reported (7). Fractional inhibition was calculated relative to DMSO treated cells (7). STAT1/STAT3 phosphorylation was quantified as previously described (53).

Enzyme-linked immunosorbent assays

IL-2 and IL-10 were detected by sandwich ELISA per manufacturer's protocol (Biolegend, San Diego, CA). Quantitation was based on absorbance at 450 nm, read on a Versamax micro-plate reader (Molecular Devices, San Jose, CA). Samples were run in triplicate.

RNP complexing

RNPs were generated by mixing a 1:2 ratio of Cas9 protein (Aldeverion, Fargo, ND) and sgRNA (Synthego, Menlo Park, CA) with gentle swirling, and incubating at 37°C for 15 minutes. Guides used were IGHA1/2: GAAGACCUUGGGGCUGG; CDK8: CUCAUGCUGAUAGGAAG.

CRISPR-Cas9 gene editing

CRISPR-Cas9 gene editing was performed as previously described (54). Briefly, human $CD4^+CD45RA^+$ naïve T cells were cultured on 96 well plates pre-coated with anti-CD3 and anti-CD28 in Xvivo 15 (Lonza, Basel, Switzerland) supplemented with 5% Fetal Bovine Serum, 50 mM 2-mercaptoethanol (Thermo Fisher, Waltham, MA), 10 mM N-Acetyl L-Cystine (Cayman Chemical, Ann Arbor, MI), 20 ng/ml IL-2 and 2 μg/ml each of anti-IL-12, anti-IFNγ and anti-Il-4. Cells were harvested 2 days later, centrifuged (90 g for 8 minutes), resuspended in buffer T, mixed with 20μM RNP and electroporated (1400 volts, 10 ms, 3 pulses) using a Neon transfection system (Thermo Fisher, Waltham, MA). Cells were transferred into 90 μl Opti-MEM (Thermo Fisher, Waltham, MA) pre-warmed to 37°C. After 24 hours, cells were fed with media supplemented with 100 ng/ml IL-2 and 1 ng/ml TGFβ. Cells were maintained for 5 additional days at a density of $1x10^6$/ml and then analyzed by flow cytometry.

In vitro proliferation and T_{reg} suppression assay

These were performed as previously described (55). Briefly, sorted $CD45.1^+CD4^+CD62L^+$ $T_{responders}$ were labeled with CellTrace Far Red (Thermo Fisher, Waltham, MA) per manufacturer's protocol and plated at $5x10^4$ cells per well in 96-well U-bottom plates in the presence of anti-CD3 anti-CD28 beads (Dynabead, Grand Island, NY). For T_{reg} suppression assays, $T_{responders}$ were co-cultured with sorted $CD45.2^+Foxp3^{IRES\text{-}GFP+}$ T_{reg} cells generated as indicated. Cells were analyzed by flow cytometry 3 days later.

T_{reg} suppression – Type 1 diabetes model

These were performed as previously described (7). Briefly, $5x10^4$ sorted $CD4^+CD62L^+$ naïve T cells isolated from NOD-*BDC2.5*$^+$ mice were injected intravenously into NOD-*scid* mice with or without $1x10^5$ T_{reg} cells generated from NOD-*BDC2.5*$^+$*FOXP3*$^{IRES\text{-}GFP}$ mice as indicated (32, 33). Blood glucose levels were monitored with a handheld Contour glucometer (Bayer, Leverkusen,

Germany) at days 3, 6, 8 and every day following. Diabetes was diagnosed when blood sugar exceeded 250 mg/dl for 2 consecutive days.

T_{reg} suppression – CD45RB^{hi} colitis model

As previously described 5x10^5 sorted CD4$^+$CD62L$^+$ naïve T cells isolated from CD45.1$^+$ mice were injected intravenously into B10-*Rag2*$^{-/-}$ mice (35, 36). 5 days later, mice were injected with either PBS or 1.5x10^5 T_{reg} cells generated from Foxp3$^{IRES-GFP}$ mice as indicated (36). Mice were monitored at least weekly for weight loss and morbidity per protocol. Mice were euthanized after 4 weeks and proximal, medial, and distal colon analyzed histologically by blinded observers as previously described (56).

Histology

Tissues were preserved in 10% formalin. Paraffin embedding, sectioning and staining with hematoxylin and eosin was performed by the Histology Core (Benaroya Research Institute, Seattle, WA).

Western Blotting

Cells were washed in PBS and lysed in either TNN lysis buffer, pH 8 (100 mM TRIS-HCl, 100 mM NaCl, 1% NP-40, 1 mM DTT, 10 mM NaF) or RIPA lysis buffer (150 mM NaCl, 1% Triton X-100, 0.5% sodium deoxycholate, 0.1% SDS, 50 mM TRIS-HCl at pH7.8) supplemented with DTT, protease inhibitors (Roche, Indianapolis, IN) and phosphatase inhibitors (Cell Signaling Technologies, Danvers, MA). Lysates were separated by SDS-PAGE using Tris-Glycine gels loaded with about 1x10^6 cell equivalents per well and transferred onto PDVF membrane (Millipore, Burlington, MA). Blots were blocked in either 5% Milk (Nestle, Vervey, Switzerland) or bovine serum albumin (Sigma Aldrich, St. Louis, MO) and visualized with Western Lightning Plus-ECL (Perkin Elmer, Waltham, MA) and/or SuperSignal West Femto substrate (Thermo Scientific, Waltham, MA) per manufacturer's instructions. Nuclear isolation was performed using Nuclei EZ Prep kit per manufacturer's instructions (Sigma Aldrich, St. Louis, MO). Fractions were subsequently lysed with Triton X-100 lysis buffer (1% Triton X-100, 150 mM NaCl, 50 mM Tris-HCl pH7.8). Band intensity was quantified by ImageJ (57). Antibodies are listed in Supplementary File 1.

RNA Isolation and qRT-PCR

RNA was isolated using RNeasy kits (Qiagen, Valencia, CA) and cDNA generated using iScript cDNA synthesis kits (BioRad, Hercules, CA) per manufacturer's directions. Real-time PCR was performed using an ABI 7500 FAST REAL-TIME PCR (Applied Biosystems, Foster City, CA) system. Cycling conditions were as follows; 1 cycle of 50°C for 2 minutes, 95°C for 10 minutes, followed by 40 cycles of 95°C for 15 seconds, and 60°C for 1 minute. Primers used were *Il17*: TTTAACTCCCTTGGCGCAAAA and CTTTCCCTCCGCATTGACAC; *Il22*: CATGCAGGAGGTGGTACCTT and CAGACGCAAGCATTTCTCAG; *Batf*: GACACAGAAAGCCGACACC and AGCACAGGGGCTCGTG; *Pou2af1*: CACCAAGGCCATACCAGGG and GAAGCAGAAACCTCCATGTCA; *Mina*: TTTGGGTCCTTAGTAGGCTCG and CCGATCCGGTCCTCAGATT; *Foxp3: GGCCCTTCTCCAGGACAGA* and *GCTGATCATGGCTGGGTTGT; Ikzf2*: *TCACAACTATCTCCAGAATGTCAGC* and *AGGCGGTACATGGTGACTCAT*; *Ikzf4*: *CGGCATCCGGCTACCCAACG* and

AGGTCACGGATTTCATCACCTGGC; *Il2ra*: *CCACATTCAAAGCCCTCTCCTA* and *GTTTTCCCACACTTCATCTTGC; Il-2*: *TTGTGCTCCTTGTCAACAGC* and *CTGGGGAGTTTCAGGTTCCT*; *Ctla4*: *ACTCATGTACCCACCGCCATA* and *GGGCATGGTTCTGGATCAAT*; *CDK8*: *GACTATCAGCGTTCCAATCCAC* and *TAGCTGAGTATCCCATGCTGC*. *β-ACTIN*: *CACCATTGGCAATGAGCGGTTC* and *AGGTCTTTGCGGATGTCCACGT; RPS18*: *TCATCCTCCGTGAGTTCTCCA* and *AGTTCCAGCACATTTTGCGAG.*

RNA-seq library preparation and sequencing

RNA-seq libraries were generated from four *Foxp3*^{GFP} littermate mice. On day 0, 1000 naïve CD4$^+$CD62L$^+$ cells were sorted for RNA-seq. The remaining cells were cultured on plates pre-coated with anti-CD3 and anti-CD28 in T_{reg}^{low}, T_{reg}^{hi} and T_{reg}^{DCA} conditions. On day 2, 250 FOXP3$^+$ cells and 500 FOXP3$^-$ cells were sorted from cells cultured in T_{reg}^{low}, T_{reg}^{hi} and T_{reg}^{DCA} conditions. On day 4, 1000 FOXP3$^+$ cells were sorted from T_{reg}^{hi} and T_{reg}^{DCA} cultures. Cells were sorted directly into lysis buffer from the SMART-Seq v4 Ultra Low Input RNA Kit for Sequencing (Takara) and frozen until all samples were ready for simultaneous processing. Reverse transcription was performed followed by PCR amplification to generate full length amplified cDNA. Sequencing libraries were constructed using the NexteraXT DNA sample preparation kit (Illumina) to generate Illumina-compatible barcoded libraries. Libraries were pooled and quantified using a Qubit® Fluorometer (Life Technologies). Dual-index, single-read sequencing of pooled libraries was carried out on a HiSeq2500 sequencer (Illumina) with 58-base reads, using HiSeq v4 Cluster and SBS kits (Illumina) with a target depth of 5 million reads per sample.

Base-calling was performed automatically by Illumina real time analysis software. Demultiplexing to generate FASTQ files was performed by bcl2fastq running on the Illumina BaseSpace platform. Subsequent processing was performed using the Galaxy platform. FASTQ reads were trimmed in two steps: 1) hard-trimming to remove 1 3'-end base (FASTQ Trimmer tool, v.1.0.0); 2) quality trimming from both ends until minimum base quality for each read ≥ 30 (FastqMcf, v.1.1.2). Reads were aligned to the GRCm38 mouse reference genome using STAR v.2.4.2a, with gene annotations from GRCm38 Ensembl release number 91. Read counts per Ensembl gene ID were quantified using htseq-count v.0.4.1. Sequencing, alignment, and quantitation metrics were obtained for FASTQ, BAM/SAM, and count files in Galaxy using FastQC v0.11.3, Picard v1.128, Samtools v1.2, and htseq-count v.0.4.1. The raw RNA-seq data has been deposited to the Gene Expression Omnibus (GEO) with accession numbers []

PCA and Correlation Analysis

All analysis of RNA-seq data was performed in the R programming language and Rstudio environment (58-60). One library (T_{reg}^{hi} day 2 GFP$^+$) was excluded from downstream analysis due to low read quality. The libraries were normalized as a single batch via TMM normalization and the genes were filtered to include only those genes classified as protein coding by Ensembl gene annotations with ≥ 5 normalized counts in ≥ 10% of the 36 libraries analyzed. Principal component analysis (PCA) was performed using the counts of the filtered gene set. Differentially expressed genes were identified using lmfits and voom WithQualityWeights from the limma package with thresholds of $\log_2$ fold change ≥ 1.5 and FDR adjusted p-value ≤ 0.05.

The R code for all analyses performed in this manuscript has been annotated and deposited as open-source code in GitHub at []

Pathway Analysis
Pathway analysis was performed using the Gene Set Enrichment Analysis Molecular Signature Database or MSigDB v7.0 which uses the hypergeometric distribution on a background of all genes to calculate a p-value (61-63).

Statistical analyses
Statistical measures, including mean values, standard deviations, Student's t-tests, Mantel–Cox tests, Mann–Whitney tests and one-way ANOVA tests, were performed using Graphpad Prism software and R. Where appropriate, unless otherwise stated, graphs display mean ± standard deviation.

Study approval
All murine experiments were performed with the approval of the IACUC of Benaroya Research Institute (Seattle, WA). Human studies were approved by the Benaroya Research Institute's Institutional Review Board and all subjects signed written informed consent prior to inclusion in the study.

Acknowledgements
We would like to express our deep appreciation to Anne Hocking, Karen Cerosaletti, Jessica Hamerman and Daniel Campbell for helpful discussion. We would like to acknowledge Tina Polintan for editorial assistance. BK was supported by N.I.H. grant K08 DK104021.

Figure legends

Fig. 1. DCA broadly regulates differentiation of murine and human T cells. (A-B) Effect of DCA on murine naïve $CD4^+$ T cells cultured in suboptimal pro-T_{reg} or -Th2 conditions (T_{reg}^{low} and $Th2^{low}$, respectively, left), near-optimal pro-Th1 or -Th17 conditions ($Th1^{hi}$ and $Th17^{hi}$, respectively, right) or neutral Th0 conditions (B)(n = 4-12, x4 experiments). (C-D) Effect of DCA, all-trans retinoic acid (ATRA) and rapamycin (RAPA) on number (C) and percent (D) of T_{reg}s generated from murine (n =9, x4 experiments) and human (n =7-8, x3 experiments) naïve $CD4^+$ T cells. Mann-Whitney results (A-B) and Kruskal-Wallis results (C-D), * P<0.05, ** P<0.01, *** P<0.001 ****P<0.0001.

Fig. 2. DCA describes a unique chemical immunophenotype. (A) Dose-response curves showing effect of DCA, harmine and HG-9-91-01 on murine $CD4^+$ T cells cultured in T_{reg}^{low}, $Th2^{low}$, $Th1^{low}$ and $Th17^{low}$ conditions (n = 3-5, x3-5 experiments). (B) Naive murine $CD4^+$ T cell cultures showing dose-response of the CDK8 inhibitors DCA and BRD-6989 on T_{reg} differentiation (left) and culture cellularity (right) (n = 2, x2 experiments). Harmine (HAR) is included for comparison. (C) Effect of CRISPR/Cas9-mediated deletion of CDK8, compared to IgA control, on propensity of human $CD4^+$ T cells to generate T_{reg}s. (n = 6, x3 experiments). Wilcoxon matched pair analysis (C), * P<0.05, ** P<0.011, *** P<0.001 ****P<0.0001.

Fig. 3. DCA enhances differentiation of functional T_{reg}s. Suppressive function of DCA-driven T_{reg}s (blue), compared to T_{reg}^{hi}-driven T_{reg}s (red). (A) Standard in vitro suppression assay, (B) NOD.BDC2.5 model of type 1 diabetes and (C) B10.*Rag2*$^{-/-}$ model of colitis. No T_{reg} controls shown in black lines. All data representative of at least 2 independent experiments (n≥4 mice per cohort). Mantel-Cox (B) and Mann-Whitney (C) results, * P<0.05, ** P<0.011, *** P<0.001 ****P<0.0001.

Fig. 4. DCA does not regulate T cell differentiation by attenuating Ser727 phosphorylation of STAT1 or STAT3. (A) Effect of DCA on IL-6-induced $STAT3^{Ser727}$ phosphorylation in unstimulated murine $CD4^+$ T cells. (B) Effect of DCA on IL-6-induced phospho-$STAT3^{Tyr705}$ and total STAT3 in stimulated murine T cells (representative of 2 independent experiments). (C) Effect of DCA on RORγt in cells cultured in $Th17^{hl}$ conditions (representative of 3 independent experiments). (D-E) Effect of DCA on Th17 (D) and T_{reg} (E) differentiation in *STAT3*^{Ser727Ala} naïve $CD4^+$ T cells. (n = 4, x2 experiments). (F) Effect of DCA on IFNγ-induced $STAT1^{Ser727}$ phosphorylation in unstimulated murine $CD4^+$ T cells (representative of 2 independent experiments). (G) Effect of DCA on IFNγ-induced phospho-$STAT1^{Tyr705}$ and total STAT1 in stimulated murine T cells (representative of 2 independent experiments). (H) Effect of DCA on T-bet in cells cultured in $Th1^{hl}$ conditions (n = 3, x3 experiments). (I-J) Effect of DCA on Th1 (I) and T_{reg} (J) differentiation in *STAT1*^{Ser727Ala} naïve $CD4^+$ T cells. (n = 4, x2 experiments). Mann-Whitney * P<0.05, ** P<0.011, *** P<0.001 ****P<0.0001.

Fig. 5. DCA enhances expression core T_{reg} transcription factors that work through multiple cis-regulatory elements. (A) Effect of DCA on expression of FOXP3-regulated genes in murine $CD4^+$ T cells cultured for 2 days in T_{reg}^{low} conditions (n = 9, x3 experiments). (B) Effect of DCA on T_{reg}

differentiation in cells lacking FOXP3 regulatory elements CNS1, CNS2 or CNS3 (n = 2, x2 experiments). Mann-Whitney (A) * P<0.05, ** P<0.011, *** P<0.001 ****P<0.0001.

Fig. 6. DCA drives novel early *Foxp3* expression via effects on c-Jun phosphorylation. (A) Timecourse of FOXP3 expression in murine $CD4^+$ T cells cultured in T_{reg}^{low}, T_{reg}^{DCA} and T_{reg}^{hi} conditions (n = 10, x5 experiments). Red arrows denote source samples for RNAseq. (B-C) Principle component (PC) analyses of samples generated in (A) (n = 4 per cohort). (D) Volcano plot comparing global gene expression in sorted day 4 $FOXP3^+$ T_{reg}s generated in T_{reg}^{DCA} or T_{reg}^{hi} conditions. Number of genes more highly expressed in T_{reg}^{DCA} or T_{reg}^{hi} T_{reg}s is indicated. (E) Transcription factor binding site enrichment analyses of genes differentially regulated by DCA in all cellular subsets analyzed show distribution across different subsets, with AP-1 as the sole common factor. (F) Effect of DCA on c-Jun phosphorylation at Ser243 and Ser63 (n = 3).

Supplemental Fig. 1. DCA enhances differentiation, not proliferation, of murine T_{reg}s. (A) Effect of DCA on T_{reg} differentiation/proliferation in sorted naïve $CD4^+$ T cells (left) and T_{reg}s (right) (≥4, x4 experiments). (B) Quantitation of *CDK8* knockdown in human CRISPR/Cas9 experiments (n = 6, x3 experiments).

Supplemental Fig. 2. CDK8 inhibition does not impact canonical pathways of T_{reg} differentiation. (A) Effect of DCA on phosphorylation of SMAD and SMAD3. (≥2 independent experiments) (B) Effect of DCA on mTOR activity, as assessed by phosphorylation of S6K and S6. (A-B) Numbers in Western blot analyses show fraction of protein phosphorylated normalized to T_{reg}^{low} conditions (representative of at least 2 experiments). (C) Ability of DCA to enhance T_{reg} differentiation in cells lacking CNS1, CNS2 or CNS3, relative to the maximal enhancement in wild-type cells. (representative of 2 independent experiments)

Supplemental Fig. 3. Expression profiling of cells cultured in various pro-T_{reg} conditions. (A) Volcano plots comparing cells cultured in either T_{reg}^{low} or T_{reg}^{hi} conditions for 2 days, separately sorted into $FOXP3^+$ and $FOXP3^-$ subsets for RNAseq. (B) Volcano plots comparing cells cultured in either T_{reg}^{DCA} or T_{reg}^{hi} conditions for 2 days, separately sorted into $FOXP3^+$ and $FOXP3^-$ subsets for RNAseq. (A-B) numbers enumerate differentially expressed genes.

References

1. Zigmond E et al. Ly6C hi monocytes in the inflamed colon give rise to proinflammatory effector cells and migratory antigen-presenting cells. *Immunity* 2012;37(6):1076–1090.

2. Zigmond E, Jung S. Intestinal macrophages: well educated exceptions from the rule. *Trends Immunol* 2013;34(4):162–168.

3. Josefowicz SZ, Lu L-F, Rudensky AY. Regulatory T cells: mechanisms of differentiation and function. *Annu. Rev. Immunol.* 2012;30:531–564.

4. Cretney E, Kallies A, Nutt SL. Differentiation and function of Foxp3(+) effector regulatory T cells. *Trends Immunol* 2013;34(2):74–80.

5. O'shea JJ, Paul WE. Mechanisms Underlying Lineage Commitment and Plasticity of Helper CD4+ T Cells. *Science* 2010;327(5969):1098–1102.

6. Batlle E, Massagué J. Transforming Growth Factor-β Signaling in Immunity and Cancer. *Immunity* 2019;50(4):924–940.

7. Khor B et al. The kinase DYRK1A reciprocally regulates the differentiation of Th17 and regulatory T cells. *Elife* 2015;4. doi:10.7554/eLife.05920

8. Sundberg TB et al. Small-molecule screening identifies inhibition of salt-inducible kinases as a therapeutic strategy to enhance immunoregulatory functions of dendritic cells. *Proc Natl Acad Sci USA* [published online ahead of print: August 11, 2014]; doi:10.1073/pnas.1412308111

9. Shi J et al. Scalable synthesis of cortistatin A and related structures. *J Am Chem Soc* 2011;133(20):8014–8027.

10. Pelish HE et al. Mediator kinase inhibition further activates super-enhancer-associated genes in AML. *Nature* 2015;526(7572):273–276.

11. Johannessen L et al. Small-molecule studies identify CDK8 as a regulator of IL-10 in myeloid cells. *Nat. Chem. Biol.* 2017;13(10):1102–1108.

12. Conaway RC, Conaway JW. Function and regulation of the Mediator complex. *Curr Opin Genet Dev* 2011;21(2):225–230.

13. Sato S et al. A set of consensus mammalian mediator subunits identified by multidimensional protein identification technology. *Mol Cell* 2004;14(5):685–691.

14. Malumbres M. Cyclin-dependent kinases. *Genome Biol* 2014;15(6):122.

15. CDK8 Kinase Activity Promotes Glycolysis. *CellReports* 2017;21(6):1495–1506.

16. Bancerek J et al. CDK8 kinase phosphorylates transcription factor STAT1 to selectively regulate the interferon response. *Immunity* 2013;38(2):250–262.

17. Lin A et al. Casein kinase II is a negative regulator of c-Jun DNA binding and AP-1 activity. *Cell* 1992;70(5):777–789.

18. Huang C-C et al. Calcineurin-mediated dephosphorylation of c-Jun Ser-243 is required for c-Jun protein stability and cell transformation. *Oncogene* 2008;27(17):2422–2429.

19. Taira N et al. DYRK2 priming phosphorylation of c-Jun and c-Myc modulates cell cycle progression in human cancer cells. *J Clin Invest* 2012;122(3):859–872.

20. Witalisz-Siepracka A et al. NK Cell-Specific CDK8 Deletion Enhances Antitumor Responses. *Cancer Immunol Res* 2018;6(4):458–466.

21. Putz EM et al. CDK8-mediated STAT1-S727 phosphorylation restrains NK cell cytotoxicity and tumor surveillance. *CellReports* 2013;4(3):437–444.

22. Guo Z, Wang G, Lv Y, Wan YY, Zheng J. Inhibition of Cdk8/Cdk19 Activity Promotes Treg Cell Differentiation and Suppresses Autoimmune Diseases. *Front Immunol* 2019;10:775–10.

23. Akamatsu M et al. Conversion of antigen-specific effector/memory T cells into Foxp3-expressing Treg cells by inhibition of CDK8/19. *Sci Immunol* 2019;4(40):eaaw2707.

24. Chen M et al. Systemic Toxicity Reported for CDK8/19 Inhibitors CCT251921 and MSC2530818 Is Not Due to Target Inhibition. *Cells* 2019;8(11):1413.

25. Coombes JL et al. A functionally specialized population of mucosal CD103+ DCs induces Foxp3+ regulatory T cells via a TGF-beta and retinoic acid-dependent mechanism. *J Exp Med* 2007;204(8):1757–1764.

26. Mucida D et al. Reciprocal TH17 and regulatory T cell differentiation mediated by retinoic acid. *Science* 2007;317(5835):256–260.

27. Sun CM et al. Small intestine lamina propria dendritic cells promote de novo generation of Foxp3 T reg cells via retinoic acid. *J Exp Med* 2007;204(8):1775–1785.

28. Haxhinasto S, Mathis D, Benoist C. The AKT-mTOR axis regulates de novo differentiation of CD4+Foxp3+ cells. *J Exp Med* 2008;205(3):565–574.

29. Hill JA et al. Retinoic acid enhances Foxp3 induction indirectly by relieving inhibition from CD4+CD44hi Cells. *Immunity* 2008;29(5):758–770.

30. Sauer S et al. T cell receptor signaling controls Foxp3 expression via PI3K, Akt, and mTOR. *Proc Natl Acad Sci USA* 2008;105(22):7797–7802.

31. Hall JA et al. Essential role for retinoic acid in the promotion of CD4(+) T cell effector responses via retinoic acid receptor alpha. *Immunity* 2011;34(3):435–447.

32. Herman AE, Freeman GJ, Mathis D, Benoist C. CD4+CD25+ T regulatory cells dependent on ICOS promote regulation of effector cells in the prediabetic lesion. *J Exp Med* 2004;199(11):1479–1489.

33. Tarbell KV, Yamazaki S, Olson K, Toy P, Steinman RM. CD25+ CD4+ T cells, expanded with dendritic cells presenting a single autoantigenic peptide, suppress autoimmune diabetes. *J Exp Med* 2004;199(11):1467–1477.

34. Powrie F, Leach MW, Mauze S, Caddle LB, Coffman RL. Phenotypically distinct subsets of CD4+ T cells induce or protect from chronic intestinal inflammation in C. B-17 scid mice. *Int Immunol* 1993;5(11):1461–1471.

35. Valatas V et al. Host-dependent control of early regulatory and effector T-cell differentiation underlies the genetic susceptibility of RAG2-deficient mouse strains to transfer colitis. *Mucosal immunology* 2013;6(3):601–611.

36. Smith PM et al. The microbial metabolites, short-chain fatty acids, regulate colonic Treg cell homeostasis. *Science* 2013;341(6145):569–573.

37. Kovarik P et al. Specificity of signaling by STAT1 depends on SH2 and C-terminal domains that regulate Ser727 phosphorylation, differentially affecting specific target gene expression. *EMBO J* 2001;20(1-2):91–100.

38. Shen Y et al. Essential role of STAT3 in postnatal survival and growth revealed by mice lacking STAT3 serine 727 phosphorylation. *Mol Cell Biol* 2004;24(1):407–419.

39. Varinou L et al. Phosphorylation of the Stat1 transactivation domain is required for full-fledged IFN-gamma-dependent innate immunity. *Immunity* 2003;19(6):793–802.

40. Wen Z, Zhong Z, Darnell JE. Maximal activation of transcription by Stat1 and Stat3 requires both tyrosine and serine phosphorylation. *Cell* 1995;82(2):241–250.

41. Afkarian M et al. T-bet is a STAT1-induced regulator of IL-12R expression in naïve CD4+ T cells. *Nature Publishing Group* 2002;3(6):549–557.

42. Lighvani AA et al. T-bet is rapidly induced by interferon-gamma in lymphoid and myeloid cells. *Proc Natl Acad Sci USA* 2001;98(26):15137–15142.

43. Yang XO et al. STAT3 regulates cytokine-mediated generation of inflammatory helper T cells. *J Biol Chem* 2007;282(13):9358–9363.

44. Zheng Y et al. Genome-wide analysis of Foxp3 target genes in developing and mature regulatory T cells. *Nature* 2007;445(7130):936–940.

45. Marson A et al. Foxp3 occupancy and regulation of key target genes during T-cell stimulation. *Nature* 2007;445(7130):931–935.

46. Fu W et al. A multiply redundant genetic switch “locks in” the transcriptional signature of regulatory T cells. *Nat Immunol* 2012;13(10):972–980.

47. Hori S, Nomura T, Sakaguchi S. Control of regulatory T cell development by the transcription factor Foxp3. *Science* 2003;299(5609):1057–1061.

48. Zheng Y et al. Role of conserved non-coding DNA elements in the Foxp3 gene in regulatory T-cell fate. *Nature* 2010;463(7282):808–812.

49. Menzl I, Witalisz-Siepracka A, Sexl V. CDK8-Novel Therapeutic Opportunities. *Pharmaceuticals* 2019;12(2):92–12.

50. Firestein R et al. CDK8 is a colorectal cancer oncogene that regulates beta-catenin activity. *Nature* 2008;455(7212):547–551.

51. Clarke PA et al. Assessing the mechanism and therapeutic potential of modulators of the human Mediator complex-associated protein kinases. *Elife* 2016;5. doi:10.7554/eLife.20722

52. Shi J et al. Stereodivergent synthesis of 17-alpha and 17-beta-alpharyl steroids: application and biological evaluation of D-ring cortistatin analogues. *Angew. Chem. Int. Ed. Engl.* 2009;48(24):4328–4331.

53. Chaudhry A et al. Interleukin-10 signaling in regulatory T cells is required for suppression of Th17 cell-mediated inflammation. *Immunity* 2011;34(4):566–578.

54. Roth TL et al. Reprogramming human T cell function and specificity with non-viral genome targeting. *Nature* 2018;559(7714):405.

55. Collison LW, Vignali DAA. In vitro Treg suppression assays. *Methods Mol Biol* 2011;707:21–37.

56. De Jong YP et al. Chronic murine colitis is dependent on the CD154/CD40 pathway and can be attenuated by anti-CD154 administration. *Gastroenterology* 2000;119(3):715–723.

57. Schneider CA, Rasband WS, Eliceiri KW. NIH Image to ImageJ: 25 years of image analysis. *Nat Methods* 2012;9(7):671–675.

58. Ritchie ME et al. limma powers differential expression analyses for RNA-sequencing and microarray studies. *Nucleic Acids Res* 2015;43(7):e47.

59. Durinck S et al. BioMart and Bioconductor: a powerful link between biological databases and microarray data analysis. *Bioinformatics* 2005;21(16):3439–3440.

60. Wickham H. *ggplot2*. Springer Science & Business Media; 2009:

61. Subramanian A et al. Gene set enrichment analysis: a knowledge-based approach for interpreting genome-wide expression profiles. *Proc Natl Acad Sci USA* 2005;102(43):15545–15550.

62. Liberzon A et al. The Molecular Signatures Database (MSigDB) hallmark gene set collection. *Cell Systems* 2015;1(6):417–425.

63. Xie X et al. Systematic discovery of regulatory motifs in human promoters and 3' UTRs by comparison of several mammals. *Nature* 2005;434(7031):338–345.

Fig. 1

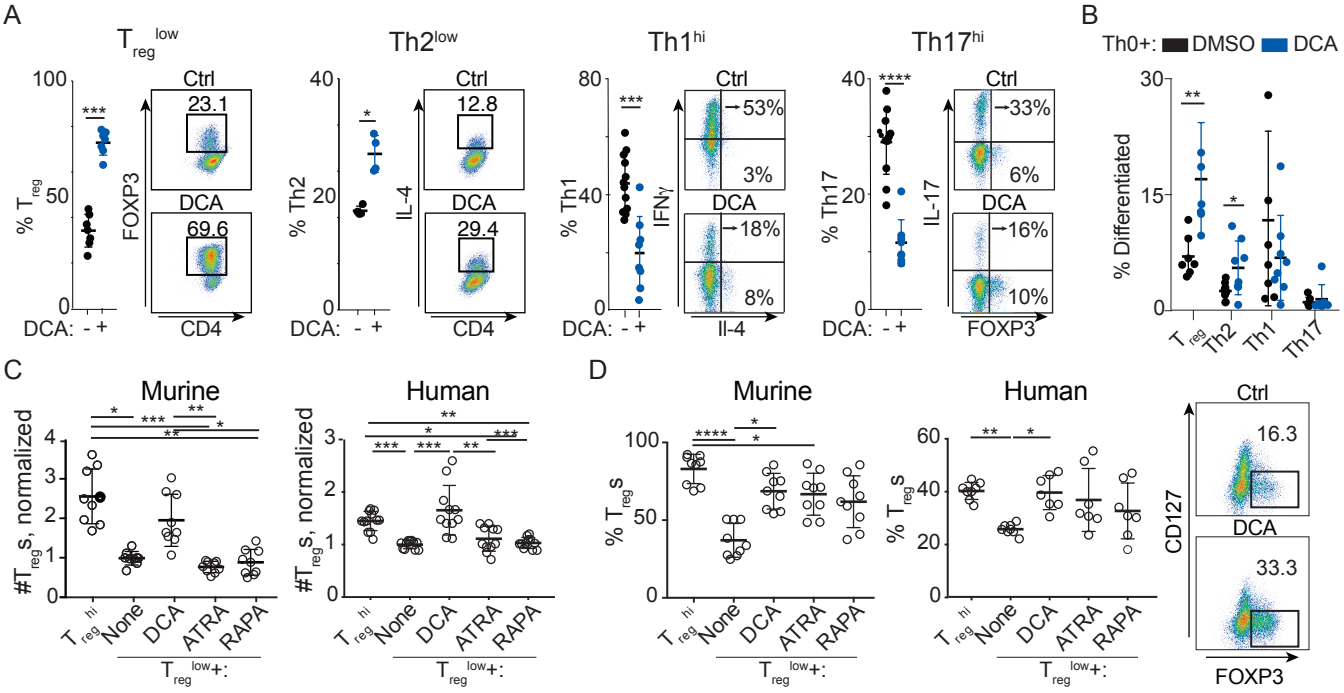

Fig. 1. DCA broadly regulates differentiation of murine and human T cells. (A-B) Effect of DCA on murine naïve CD4⁺ T cells cultured in suboptimal pro-T_{reg} or -Th2 conditions (T_{reg}^{low} and $Th2^{low}$, respectively, left), near-optimal pro-Th1 or -Th17 conditions ($Th1^{hi}$ and $Th17^{hi}$, respectively, right) or neutral Th0 conditions (B)(n = 4-12, x4 experiments). (C-D) Effect of DCA, all-trans retinoic acid (ATRA) and rapamycin (RAPA) on number (C) and percent (D) of T_{reg}s generated from murine (n =9, x4 experiments) and human (n =7-8, x3 experiments) naïve CD4⁺ T cells. Mann-Whitney results (A-B) and Kruskal-Wallis results (C-D), * P<0.05, ** P<0.01, *** P<0.001 ****P<0.0001.

Fig. 2

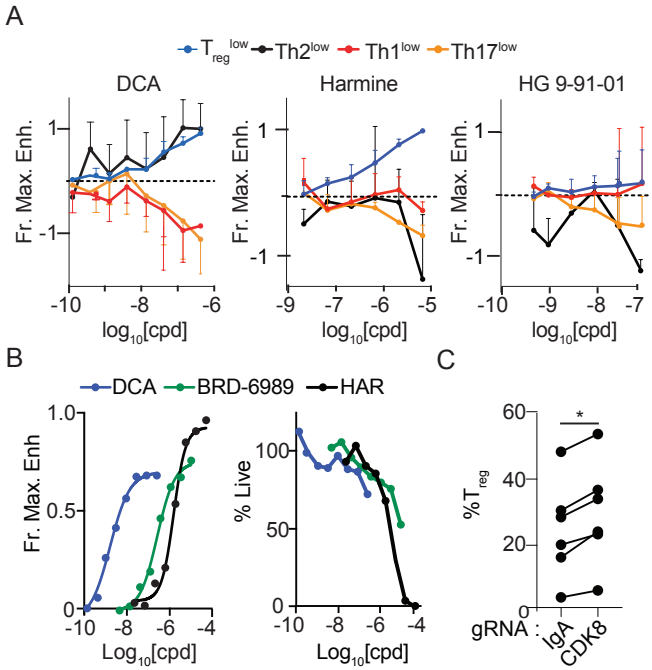

Fig. 2. DCA describes a unique chemical immuno-phenotype. (A) Dose-response curves showing effect of DCA, harmine and HG-9-91-01 on murine CD4⁺ T cells cultured in T_{reg}^{low}, $Th2^{low}$, $Th1^{low}$ and $Th17^{low}$ conditions (n = 3-5, x3-5 experiments). (B) Naive murine CD4⁺ T cell cultures showing dose-response of the CDK8 inhibitors DCA and BRD-6989 on T_{reg} differentiation (left) and culture cellularity (right) (n = 2, x2 experiments). Harmine (HAR) is included for comparison. (C) Effect of CRISPR/Cas9-mediated deletion of CDK8, compared to IgA control, on propensity of human CD4⁺ T cells to generate T_{reg}s. (n = 6, x3 experiments). Wilcoxon matched pair analysis (C), * P<0.05, ** P<0.011, *** P<0.001 ****P<0.0001.

Fig. 3

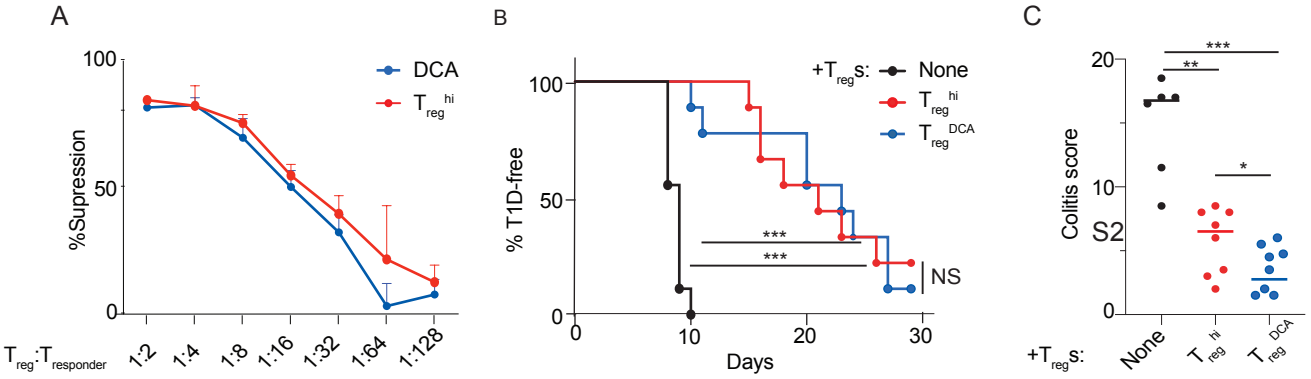

Fig. 3. DCA enhances differentiation of functional T_{reg}s. Suppressive function of DCA-driven T_{reg}s (blue), compared to T_{reg}^{hi}-driven T_{reg}s (red). (A) Standard in vitro suppression assay, (B) NOD.BDC2.5 model of type 1 diabetes and (C) B10 RAG2$^{-/-}$ model of colitis. No T_{reg} controls shown in black lines. All data representative of at least 2 independent experiments (n≥4 mice per cohort). Mantel-Cox (B) and Mann-Whitney (C) results, * P<0.05, ** P<0.011, *** P<0.001 ****P<0.0001.

Fig. 4

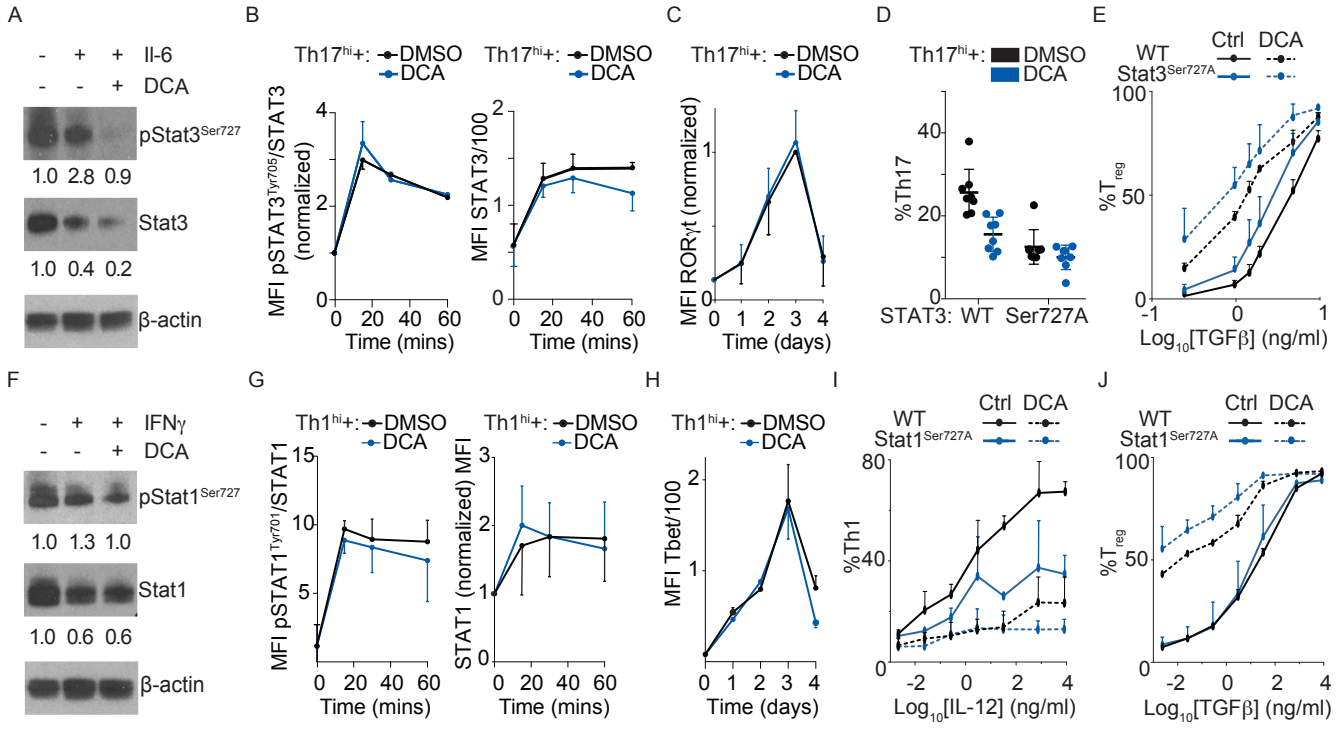

Fig. 4. DCA does not regulate T cell differentiation by attenuating Ser727 phosphorylation of STAT1 or STAT3. (A) Effect of DCA on IL-6-induced STAT3^{Ser727} phosphorylation in unstimulated murine CD4^{+} T cells. (B) Effect of DCA on IL-6-induced phospho-STAT3^{Tyr705} and total STAT3 in stimulated murine T cells (representative of 2 independent experiments). (C) Effect of DCA on RORγt in cells cultured in Th17^{hi} conditions (representative of 3 independent experiments). (D-E) Effect of DCA on Th17 (D) and T_{reg} (E) differentiation in STAT3^{Ser727Ala} naïve CD4^{+} T cells. (n = 4, x2 experiments). (F) Effect of DCA on IFNγ–induced STAT1^{Ser727} phosphorylation in unstimulated murine CD4^{+} T cells (representative of 2 independent experiments). (G) Effect of DCA on IFNγ-induced phospho-STAT1^{Tyr705} and total STAT1 in stimulated murine T cells (representative of 2 independent experiments). (H) Effect of DCA on T-bet in cells cultured in Th1^{hi} conditions (n = 3, x3 experiments). (I-J) Effect of DCA on Th1 (I) and T_{reg} (J) differentiation in STAT1^{Ser727Ala} naïve CD4^{+} T cells. (n = 4, x2 experiments). Mann-Whitney * P<0.05, ** P<0.011, *** P<0.001 ****P<0.0001.

Fig. 5

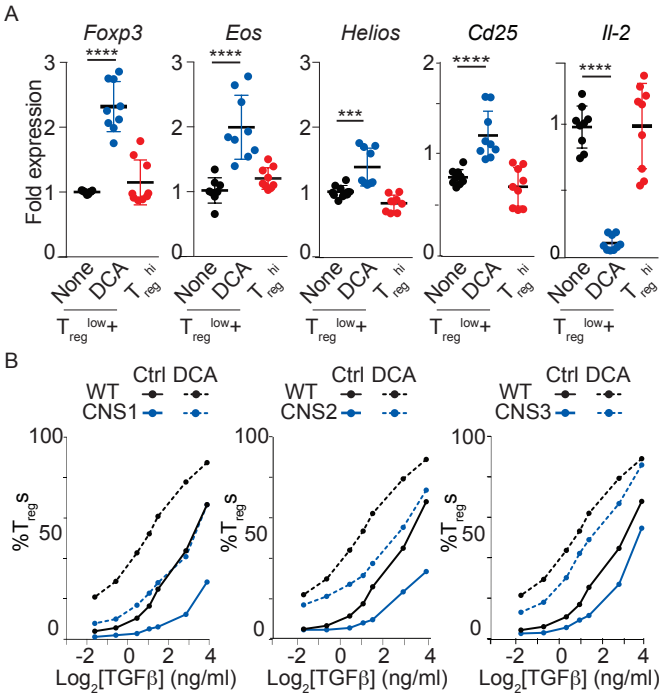

Fig. 5. DCA enhances expression core T_{reg} transcription factors that work through multiple cis-regulatory elements. (A) Effect of DCA on expression of FOXP3-regulated genes in murine $CD4^+$ T cells cultured for 2 days in T_{reg}^{low} conditions (n = 9, x3 experiments). (B) Effect of DCA on T_{reg} differentiation in cells lacking FOXP3 regulatory elements CNS1, CNS2 or CNS3 (n = 2, x2 experiments). Mann-Whitney (A) * P<0.05, ** P<0.011, *** P<0.001 ****P<0.0001.

Fig. 6

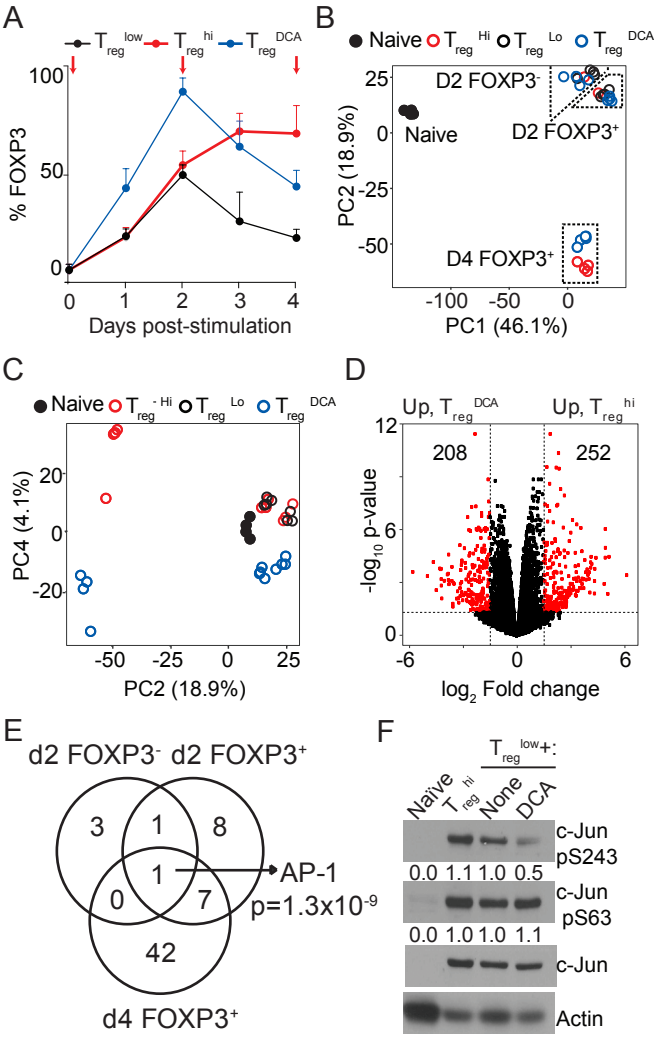

Fig. 6. DCA drives novel early Foxp3 expression via effects on c-Jun phosphorylation. (A) Time-course of FOXP3 expression in murine CD4+ T cells cultured in T_{reg}^{low}, T_{reg}^{DCA} and T_{reg}^{hi} conditions (n = 10, x5 experiments). Red arrows denote source samples for RNAseq. (B-C) Principle component (PC) analyses of samples generated in (A) (n = 4 per cohort). (D) Volcano plot comparing global gene expression in sorted day 4 FOXP3+ T_{reg}s generated in T_{reg}^{DCA} or T_{reg}^{hi} conditions. Number of genes more highly expressed in T_{reg}^{DCA} or T_{reg}^{hi} T_{reg}s is indicated. (E) Transcription factor binding site enrichment analyses of genes differentially regulated by DCA in all cellular subsets analyzed show distribution across different subsets, with AP-1 as the sole common factor. (F) Effect of DCA on c-Jun phosphorylation at Ser243 and Ser63 (n = 3).